Quantum electrodynamics of a nanocavity coupled with exciton complexes in a quantum dot

Makoto Yamaguchi, Takashi Asano, Kazunobu Kojima, and Susumu Noda
Department of Electronic Science and Engineering, Kyoto University, Katsura, Nishikyo-ku, Kyoto 615-8510, Japan
(Received 17 April 2009; revised manuscript received 16 July 2009; published 26 October 2009)

A comprehensive theory of the coupling between a nanocavity and exciton complexes in a quantum dot is developed, which successfully predicts the spectral triplet in the strong coupling regime that has been observed in several experiments but, which is unexpected according to conventional cavity quantum electrodynamics. The quantum anti-Zeno effect is found to play an essential role in the appearance of the central peak in the triplet under a low-excitation regime. The effect of hyperfine interactions is also discussed, which results in the cavity-mediated mixing of bright and dark exciton states. These results provide significant new insight into solid-state cavity quantum electrodynamics.

DOI: 10.1103/PhysRevB.80.155326 PACS number(s): 78.67.Hc, 42.50.Pq, 73.21.La, 78.67.De

I. INTRODUCTION

The coupled system consisting of a nanocavity and a quantum dot (QD) has been extensively investigated in the past few years because it has promising properties for applications such as quantum information processing (QIP),[1] single photon sources,[2] and ultimately low-threshold lasers.[3] In this system the following two phenomena are expected to occur naturally, analogous to the atomic systems in cavity quantum electrodynamics (QED): first, light should be emitted only at the QD transition energy under off-resonant conditions; second, vacuum Rabi splitting (VRS) should occur under on-resonant conditions. However, experimental reports have shown clear deviations from these features. First, light emission from the cavity occurs even when it is largely detuned from the QD.[4–13] Second, spectral triplets are formed by additional bare cavity lines between the VRS lines under on-resonant conditions.[7,10,11] These features are unique to semiconductor systems and are not predicted by conventional cavity QED in atomic systems. Recently, we reported that the quantum anti-Zeno effect (AZE), induced by pure dephasing in the QD, plays a key role in off-resonant cavity light emission.[14,15] In our previous study the QD was modeled by a simple two-level system (TLS) and the effect of pure dephasing (or nonreferred measurements) was explained as follows: it broadens the transition energy of the TLS, which makes it possible for the tail of the transition energy to overlap with the cavity energy, and generates an additional way in which to interact with the cavity. Because of this interaction, a cavity photon is created with the transition of the excited TLS to the ground state, a process generally known as the AZE. This effect seems to be negligible in most cases, because the tail of the TLS transition energy at the cavity energy is so weak that the interaction is not sufficiently large to overcome the direct spontaneous emission from the TLS to free space. However, the unique situation achieved in semiconductor nanocavity QED systems strongly enhances the AZE, resulting in off-resonant cavity light emission for the following reasons. First, the coupling constant between the cavity and the TLS is huge due to the small cavity volume. Second, the quality factor (Q factor) of the cavity is relatively large. Third, direct spontaneous emission from the TLS to free space is strongly suppressed due to the in-plane photonic band-gap (PBG) effect[16,17] in the case of the two-dimensional photonic crystal (2DPC) nanocavities[18] shown in Fig. 1(a). These features are well described by a factor F, presented in Ref. 15, which expresses the ratio of the integrated intensity at the cavity energy to that at the TLS energy as $F:(1-F)$. Here, F is given by

$$F \approx \frac{\Gamma_{\mathrm{spon}} + \gamma_{\mathrm{phase}}}{\Gamma_{\mathrm{spon}}(\delta\omega_{\mathrm{TLS,cav}}/g_{\mathrm{TLS,cav}})^2 + \Gamma_{\mathrm{cav}} + (\Gamma_{\mathrm{spon}} + \gamma_{\mathrm{phase}})}, \tag{1}$$

where $2\Gamma_{\mathrm{spon}}$ is the direct spontaneous emission rate of the TLS to free space, $2\Gamma_{\mathrm{cav}}$ is the optical damping rate of the cavity (which is determined by its Q factor), $2\gamma_{\mathrm{phase}}$ is the pure dephasing rate of the TLS, $\delta\omega_{\mathrm{TLS,cav}}$ is the detuning of the TLS from the cavity, and $g_{\mathrm{TLS,cav}}$ is the coupling constant between the TLS and the cavity.

Thus, the off-resonant cavity light emission can successfully be explained by this nanocavity-enhanced AZE, and we have derived the fundamental expression that describes this phenomenon. An equivalent analysis was also reported independently by another group.[19] However, arriving at a full description of the entire emission mechanism, including the on-resonant spectral triplet, remains a puzzling problem. Furthermore, recent experiments[10] have revealed unique cou-

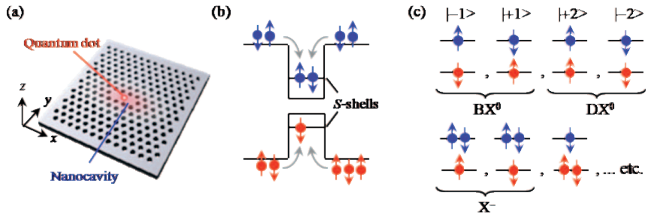

FIG. 1. (Color) Schematic illustration of the system considered. (a) QD embedded in a 2DPC nanocavity. Here, the x, y, and z directions correspond to the [110], [1–10], and [001] lattice directions, respectively. (b) First confined levels (S shell) in the QD. (c) Examples of different charge configurations in the S shells where the arrows represent the electron spins and heavy-hole pseudospins, respectively. Individual states in BX^0 and DX^0 are labeled by the total angular momentum of the carriers.

pling of the nanocavity with individual charging states in the QD, and have found that dark excitons (DX^0) are optically activated by cavity-mediated mixing with bright excitons (BX^0). These features are beyond the TLS model of the QD, and are not explained by any previously reported theories. It is important to clarify these emission mechanisms, because they directly influence the design and performance of relevant applications.

In this paper, we develop a comprehensive theory of the coupling between a nanocavity and a QD based on the quantum master equation (QME), in which individual charge configurations are taken into account [Figs. 1(b) and 1(c)]. We then carry out numerical calculations that not only reproduce the unique features of the QD-exciton complexes but also successfully predict the on-resonant spectral triplet. In this system, the AZE is shown to play an essential role in the appearance of the central cavity peak of the spectral triplet in combination with the charging states under a low-excitation regime. Furthermore, the cavity-mediated mixing of bright and dark exciton states is also shown to occur as a result of hyperfine (HF) interactions enhanced by the nanocavity.

A theoretical model that describes the dynamics of a nanocavity and a QD in the framework of the QME is presented in Sec. II of the present paper. Numerically calculated results that include the emission lines of individual charge configurations and a discussion of the origin of the spectral triplet and the cavity-mediated mixing are presented in Sec. III. Finally, our results are put into perspective and summarized in Sec. IV. Further details are presented in the appendices at the end of the paper.

II. THEORETICAL METHODS

In all previous studies, the spectral features of a single QD coupled with a nanocavity were treated, to the best of our knowledge, without including the various types of exciton complex in the QD.[14,15,19–22] In contrast, here we formulate a theory of exciton complexes found in QDs that are coupled with a nanocavity by taking into account individual charge configurations and their Coulomb and exchange interactions.

In our treatment, a Stranski-Krastanov indium arsenide (InAs) QD grown on a gallium arsenide (GaAs) substrate is assumed, where the x and y directions are defined as [110] and [1–10], respectively. As shown in Fig. 1(b), electrons with $S_z=\pm 1/2$ spins and heavy holes with $J_z=\pm 3/2$ pseudospins are independently injected into the first confined levels (S-shells) in the QD. Therefore, a nonequal number of electrons and heavy holes can be injected and various exciton states are formed, as shown in Fig. 1(c). This situation is usually achieved by optical excitation of the barrier region (GaAs).[23,24] The quantum dynamics in this system can be described by the QME in the interaction picture, that is,

$$\mathrm{d}\rho_S(t)/\mathrm{d}t = -\mathrm{i}\hbar^{-1}[H_S(t),\rho_S(t)] + L\rho_S(t), \tag{2}$$

which is focused on a subject system consisting of the cavity mode and the S shells in the QD. Here, $\rho_S(t)$ is a reduced density operator, $H_S(t)$ denotes interactions inside the subject system (non-Markov processes), and the Liouvillian L denotes irreversible processes (Markov processes). The basis of the states is then taken as $|i_{1/2},j_{-1/2}\rangle\otimes|k_{3/2},l_{-3/2}\rangle\otimes|p_{\mathrm{cav}}\rangle$ ($i,j,k,l=0$ or 1, $p=0,1,2,\ldots$), where $|i_{1/2},j_{-1/2}\rangle$ denotes $i(j)$ electrons with spin $+1/2$ $(-1/2)$, $|k_{3/2},l_{-3/2}\rangle$ denotes $k(l)$ heavy holes with pseudospin $+3/2$ $(-3/2)$, and $|p_{\mathrm{cav}}\rangle$ corresponds to p photons in the cavity. As a result, a total of 16 different charging states are taken into account, including not only BX^0 and DX^0 but also biexcitons (XX^0), positively (X^+) and negatively (X^-) charged excitons, and other optically inactive states. Hereafter, for descriptive convenience, each BX^0 state of $|0_{1/2},1_{-1/2}\rangle\otimes|1_{3/2},0_{-3/2}\rangle$ and $|1_{1/2},0_{-1/2}\rangle\otimes|0_{3/2},1_{-3/2}\rangle$ is labeled by $|+1\rangle$ and $|-1\rangle$, and each DX^0 state of $|1_{1/2},0_{-1/2}\rangle\otimes|1_{3/2},0_{-3/2}\rangle$ and $|0_{1/2},1_{-1/2}\rangle\otimes|0_{3/2},1_{-3/2}\rangle$ is denoted by $|+2\rangle$ and $|-2\rangle$, as shown in Fig. 1(c).

A. Non-Markov processes

We shall begin by explaining non-Markov processes expressed by

$$H_S(t) = H_{\mathrm{CL}} + H_{\mathrm{EX}} + H_{\mathrm{LM}}(t). \tag{3}$$

Here, H_{CL} and H_{EX} denote the Coulomb and exchange interactions of carriers in the S shells, respectively, and $H_{\mathrm{LM}}(t)$ denotes the light-matter coupling between the cavity and the excitons. The term H_{CL} in Eq. (3) is expressed by

$$H_{\mathrm{CL}} = J^{\mathrm{e\text{-}e}}n_\downarrow n_\uparrow + J^{\mathrm{h\text{-}h}}m_\downarrow m_\uparrow - J^{\mathrm{e\text{-}h}}(n_\downarrow + n_\uparrow)(m_\downarrow + m_\uparrow), \tag{4}$$

where $n_\sigma \equiv c_\sigma^\dagger c_\sigma$ and $m_\sigma \equiv d_\sigma^\dagger d_\sigma$ ($\sigma=\uparrow$ or $\downarrow$) are the number operators of the electrons and holes defined by the Fermi creation and annihilation operators of the electrons ($c_\sigma^\dagger, c_\sigma$) and holes ($d_\sigma^\dagger, d_\sigma$). The first term in Eq. (4) describes the Coulomb repulsion energy between two electrons with different spins characterized by $J^{\mathrm{e\text{-}e}}$. In a similar way, the second and third terms also represent the Coulomb charging energies between different carriers characterized by $J^{\mathrm{h\text{-}h}}$ and $J^{\mathrm{e\text{-}h}}$. The term H_{EX} in Eq. (3) is described by

$$H_{\mathrm{EX}} = -2\delta_0 s_{\mathrm{h}}^z s_{\mathrm{e}}^z + \delta_1(s_{\mathrm{h}}^+ s_{\mathrm{e}}^- + s_{\mathrm{h}}^- s_{\mathrm{e}}^+)/2 + \delta_2(s_{\mathrm{h}}^+ s_{\mathrm{e}}^+ + s_{\mathrm{h}}^- s_{\mathrm{e}}^-)/2, \tag{5}$$

where $s_{\mathrm{e}}^+ \equiv c_\uparrow^\dagger c_\downarrow$, $s_{\mathrm{e}}^- \equiv c_\downarrow^\dagger c_\uparrow$, and $s_{\mathrm{e}}^z \equiv (n_\uparrow - n_\downarrow)/2$ are the spin operators of electrons, and $s_{\mathrm{h}}^+ \equiv d_\uparrow^\dagger d_\downarrow$, $s_{\mathrm{h}}^- \equiv d_\downarrow^\dagger d_\uparrow$, and $s_{\mathrm{h}}^z \equiv (m_\uparrow - m_\downarrow)/2$ are the effective spin operators[25] corresponding to the two heavy-hole states $J_z=\pm 3/2$. Here, δ_0, δ_1, and δ_2 are the parameters determined by the anisotropy of the QD.[25–27] δ_0 determines the energy difference between the $|\pm 1\rangle$ and $|\pm 2\rangle$ states. In contrast, δ_1 determines the fine-structure splitting (FSS) of the $|\pm 1\rangle$ states (BX^0), and their eigenstates are mixed into $(|+1\rangle \pm |-1\rangle)/\sqrt{2}$. These modified bright states $(|+1\rangle - |-1\rangle)/\sqrt{2}$ and $(|+1\rangle + |-1\rangle)/\sqrt{2}$ are known to interact with x - and y-polarized light fields, respectively. In the same way, δ_2 determines the FSS of the $|\pm 2\rangle$ states (DX^0), and their eigenstates turn into $(|+2\rangle \pm |-2\rangle)/\sqrt{2}$. Finally, $H_{\mathrm{LM}}(t)$ is formulated by $H_{\mathrm{LM}}(t) = H_{\mathrm{LM}}^{+1}(t) + H_{\mathrm{LM}}^{-1}(t)$ with

$$H_{\mathrm{LM}}^{+1}(t) = \hbar c_\downarrow^\dagger d_\uparrow^\dagger a_{\mathrm{cav}} g_{+1} \exp(\mathrm{i}\delta\omega t) + \mathrm{H.c.}, \tag{6}$$

$$H_{\mathrm{LM}}^{-1}(t) = \hbar c_{\uparrow}^{\dagger} d_{\downarrow}^{\dagger} a_{\mathrm{cav}} g_{-1} \exp(\mathrm{i}\delta\omega t) + \mathrm{H.c.}, \tag{7}$$

where a_{cav} is the Bose annihilation operator of the cavity mode, and $\delta\omega$ is the detuning of the QD transition frequency from the cavity. We note that the two coupling constants, $g_{\pm 1}$, both depend on the polarization of the cavity at the QD and are mutually related. Given the respective Bloch functions of the conduction and heavy-hole bands, $g_{\pm 1}$ can be written as

$$g_{\pm 1} = \mp g(\cos\ \theta_{\mathrm{cav}} \mp \mathrm{i}\ \sin\ \theta_{\mathrm{cav}}), \tag{8}$$

where θ_{cav} is the angle between the cavity polarization and the x axis. The magnitude of the interaction between the cavity and each optically active state of BX^0, X^+, X^-, and XX^0 is consistently determined by this relationship. In order to understand this, it is instructive to note that $H_{\mathrm{LM}}(t)$ can be rewritten as $H_{\mathrm{LM}}(t) = H_{\mathrm{LM}}^{x}(t) + H_{\mathrm{LM}}^{y}(t)$ with

$$H_{\mathrm{LM}}^{x}(t) = \hbar\sqrt{2}\ \cos\ \theta_{\mathrm{cav}} g B_x^{\dagger} a_{\mathrm{cav}} \exp(\mathrm{i}\delta\omega\ t) + \mathrm{H.c.}, \tag{9}$$

$$H_{\mathrm{LM}}^{y}(t) = \mathrm{i}\hbar\sqrt{2}\ \sin\ \theta_{\mathrm{cav}} g B_y^{\dagger} a_{\mathrm{cav}} \exp(\mathrm{i}\delta\omega t) + \mathrm{H.c.}, \tag{10}$$

where B_x and B_y are defined as $(d_{\downarrow}c_{\uparrow} - d_{\uparrow}c_{\downarrow})/\sqrt{2}$ and $(d_{\downarrow}c_{\uparrow} + d_{\uparrow}c_{\downarrow})/\sqrt{2}$, respectively. Considering an example of $B_x^{\dagger}|\mathrm{GS}\rangle = -(|+1\rangle - |-1\rangle)/\sqrt{2}$ with $|\mathrm{GS}\rangle \equiv |0_{1/2}, 0_{-1/2}\rangle \otimes |0_{3/2}, 0_{-3/2}\rangle$, it can be understood that B_x ($B_x^{\dagger}$) represents the annihilation (creation) operator of the x-polarized BX^0 state. A similar principle applies to B_y and $B_y^{\dagger}$. Thus, the magnitude of the interaction between the cavity and each optically active state is consistently determined by the relationship expressed in Eq. (8).

B. Markov processes

Next, we discuss the Markov processes expressed by the Liouvillian, L, in Eq. (2), which can be divided into four terms:

$$L = L_{\mathrm{cav}} + L_{\mathrm{spon}} + L_{\mathrm{phase}} + L_{\mathrm{inj}}. \tag{11}$$

Here, the first term denotes the photon escape from the cavity to free space at a rate of $2\Gamma_{\mathrm{cav}}$, the second term denotes the direct photon emission from the QD to free space at a rate of $2\Gamma_{\mathrm{spon}}$, the third term denotes the pure dephasing of the electrons at a rate of $2\gamma_{\mathrm{phase}}^{\mathrm{e}}$ and heavy holes at a rate of $2\gamma_{\mathrm{phase}}^{\mathrm{h}}$, and the fourth term indicates that the electrons and holes are independently injected at an equal rate of $2P$ with random spins (pseudospins). Here, the differences in rates between the carriers and spins are neglected for simplicity. Each Liouvillian can be written in the Lindblad form as

$$L_{\mathrm{cav}}X = -\Gamma_{\mathrm{cav}}(a_{\mathrm{cav}}^{\dagger}a_{\mathrm{cav}}X + Xa_{\mathrm{cav}}^{\dagger}a_{\mathrm{cav}} - 2a_{\mathrm{cav}}Xa_{\mathrm{cav}}^{\dagger}), \tag{12}$$

$$L_{\mathrm{spon}}X = -\Gamma_{\mathrm{spon}}\sum_{\sigma}(c_{\sigma}^{\dagger}d_{-\sigma}^{\dagger}d_{-\sigma}c_{\sigma}X + Xc_{\sigma}^{\dagger}d_{-\sigma}^{\dagger}d_{-\sigma}c_{\sigma} - 2d_{-\sigma}c_{\sigma}Xc_{\sigma}^{\dagger}d_{-\sigma}^{\dagger}), \tag{13}$$

$$L_{\mathrm{phase}}X = -\gamma_{\mathrm{phase}}^{\mathrm{e}}\sum_{\sigma}(n_{\sigma}X + Xn_{\sigma} - 2n_{\sigma}Xn_{\sigma}) - \gamma_{\mathrm{phase}}^{\mathrm{h}}\sum_{\sigma}(m_{\sigma}X + Xm_{\sigma} - 2m_{\sigma}Xm_{\sigma}), \tag{14}$$

$$L_{\mathrm{inj}}X = -P\sum_{\sigma}(c_{\sigma}c_{\sigma}^{\dagger}X + Xc_{\sigma}c_{\sigma}^{\dagger} - 2c_{\sigma}^{\dagger}Xc_{\sigma}) - P\sum_{\sigma}(d_{\sigma}d_{\sigma}^{\dagger}X + Xd_{\sigma}d_{\sigma}^{\dagger} - 2d_{\sigma}^{\dagger}Xd_{\sigma}), \tag{15}$$

where $-\sigma$ denotes the inversion of σ, and the summation of σ is taken for $\uparrow$ and $\downarrow$. The term L_{cav} is the same as the commonly used Liouvillian,[14,15,20,21] whereas L_{spon} and L_{phase} are an extension of our previous work.[15] It should be noted that these two Liouvillians are able to consistently express each Markov process for various charging states at the same time. The original form of L_{phase} was initially derived as a result of Coulomb interactions with surrounding carriers,[15] but phonon-mediated pure dephasing also takes the same form under the Markov approximation, because the most important point for the derivation of L_{phase} is that the effective interaction Hamiltonian between the carriers of the QD and the environmental degrees of freedom commutes with the number operators of the carriers in the QD. The pumping model proposed by Laussy *et al.*[21] is expanded for L_{inj} in order to describe the independent injection of electrons and holes.

C. Emission spectra

Finally, we focus on the expression for the emitted photon spectrum $S(\omega)$ in the steady state, which can be divided into two terms

$$S(\omega) = S_{\mathrm{cav}}(\omega) + S_{\mathrm{spon}}(\omega). \tag{16}$$

Here, $S_{\mathrm{cav}}(\omega)$ and $S_{\mathrm{spon}}(\omega)$ denote the spectral components following the spatial radiation pattern of the cavity mode and the QD, respectively. Each spectrum is characterized by the operator that produces the corresponding Lindblad form in the Liouvillians L_{cav} and L_{spon}. Therefore, $S_{\mathrm{cav}}(\omega)$ is expressed as

$$S_{\mathrm{cav}}(\omega) = \frac{2\Gamma_{\mathrm{cav}}}{\pi}\mathrm{Re}\left[\int_0^{\infty}\mathrm{d}\tau\langle a_{\mathrm{cav}}^{\dagger}(t)a_{\mathrm{cav}}(t+\tau)\rangle \times\exp(\mathrm{i}\omega\tau - \gamma_{\mathrm{reso}}\tau)\right], \tag{17}$$

where the spectral resolution is defined by $2\gamma_{\mathrm{reso}}$. The Liouvillian L_{spon} in Eq. (13) can be rewritten using B_x and B_y as

$$L_{\mathrm{spon}}X = -\Gamma_{\mathrm{spon}}(B_x^{\dagger}B_xX + XB_x^{\dagger}B_x - 2B_xXB_x^{\dagger}) - \Gamma_{\mathrm{spon}}(B_y^{\dagger}B_yX + XB_y^{\dagger}B_y - 2B_yXB_y^{\dagger}), \tag{18}$$

where two Lindblad forms are included. Therefore, $S_{\mathrm{spon}}(\omega)$ is expressed by a sum of two linearly polarized components:

$$S_{\mathrm{spon}}(\omega) = S_x(\omega) + S_y(\omega), \tag{19}$$

with

TABLE I. Standard parameters used in this work.

Quantity	Value	Unit	Quantity	Value	Unit
$J^{e\text{-}e}$	2.6×10^{1}	meV	$2\hbar\Gamma_{cav}$	6.9×10^{1}	μeV
$J^{h\text{-}h}$	3.0×10^{1}	meV	$2\hbar\Gamma_{spon}$	4.4×10^{1}	neV
$J^{e\text{-}h}$	2.9×10^{1}	meV	$2\hbar\gamma_{phase}$	3.0×10^{1}	μeV
δ_0	2.5×10^{2}	μeV	$2\hbar P$	3.3×10^{1}	neV
δ_1	-3.0×10^{1}	μeV	$2\hbar g$	2.1×10^{2}	μeV
δ_2	-1.0×10^{1}	μeV	θ_{cav}	$\pi/2$	Rad

$$S_x(\omega) \equiv \frac{2\Gamma_{spon}}{\pi}\mathrm{Re}\left[\int_0^\infty d\tau\langle B_x^\dagger(t)B_x(t+\tau)\rangle\exp(i\omega\tau-\gamma_{reso}\tau)\right], \tag{20}$$

$$S_y(\omega) \equiv \frac{2\Gamma_{spon}}{\pi}\mathrm{Re}\left[\int_0^\infty d\tau\langle B_y^\dagger(t)B_y(t+\tau)\rangle\exp(i\omega\tau-\gamma_{reso}\tau)\right]. \tag{21}$$

Here, $S_x(\omega)$ and $S_y(\omega)$ denote the x- and y-polarized components in $S_{spon}(\omega)$. The term $S_{spon}(\omega)$ can also be divided into two circularly polarized components, as expected from the original form of L_{spon} in Eq. (13). These expressions are described in Appendix A.

III. RESULTS AND DISCUSSION

We have calculated the steady state emitted photon spectra of $S(\omega)$ by transforming the QME into differential equations of matrix elements for $\rho_S(t)$ using the quantum regression theorem.[28,29] Unless otherwise stated, the parameters listed in Table I are used here: $J^{e\text{-}e}$, $J^{h\text{-}h}$, and $J^{e\text{-}h}$ are estimated from the calculated values reported in Ref. 30, and the other parameters are consistent with experimental results[7,10,11] for a y-polarized cavity mode at the QD position ($\theta_{cav}=\pi/2$). Here, the term $2\gamma_{phase}$ is defined as $2\gamma^e_{phase}+2\gamma^h_{phase}$, and it is assumed that $2\gamma^e_{phase}=2\gamma^h_{phase}$. We note that a sufficiently low carrier injection rate is used in the calculation in order to avoid saturation of the states in the QD.

A. Spectral triplets

Figures 2(a) and 2(b) show the calculated values of $S(\omega)$ as a function of the detuning $\delta\omega$ for two different cases where the pure dephasing is either ignored ($2\gamma_{phase}=0$ μeV) or taken into consideration ($2\gamma_{phase}=30$ μeV), respectively. As shown in Fig. 2(a), there are essentially four emission lines of X^+, X^-, BX^0, and XX^0. The X^+ and X^- lines are both composed of two oppositely circularly polarized lines, whereas the BX^0 and XX^0 lines include two non degenerate linearly polarized lines in the x and y directions. When the cavity is tuned to X^+, it splits into two lines with a separation of $2\hbar g=2.1\times10^2$ μeV, corresponding to VRS. As the tuning proceeds, VRS can again be seen in resonance with BX^0 (the splitting is $2\sqrt{2}\hbar g=3.0\times10^2$ μeV). In comparison with X^+, there is one line in BX^0 that is unaffected by the cavity. This corresponds to the x-polarized state in BX^0, which cannot interact with the y-polarized cavity field. Furthermore, when the cavity is tuned to BX^0, a simultaneous splitting of XX^0 occurs because the final states of the XX^0 transitions are determined by BX^0. Again, the unaffected line in XX^0 is the x-polarized component. These features are consistent with the experimental results,[10] indicating that our treatment of the exciton complexes works well; however, the result shown in Fig. 2(a) does not reproduce the experimentally observed off-resonant cavity light emission and the on-resonant triplet (the x-polarized line in BX^0 is ruled out as the origin of the triplet because the central peak in the triplet preserves the exact wavelength, line width, and polarization of the cavity mode in the experiments). The emission spectra are drastically changed when the pure dephasing is taken into account, as shown in Fig. 2(b). Even if the cavity is detuned from all emission lines, the cavity light emission appears to be in agreement with previous reports.[14,15,19] Unexpectedly, bare cavity lines constantly appear between the VRS peaks when the cavity is tuned to X^+ and BX^0 (see the insets to Fig. 2). These features have also been observed experimentally.[7,10,11] Our results indicate that both the AZE and the practical QD model are necessary to reproduce the spectral triplet.

Unlike the TLS model, the present model allows for various charging states. However, because the QD is allowed to take only one state at a time, each optically active state is expected to act as if a simple TLS is interacting with the cavity. Therefore, one might expect the intensity of the bare cavity line to be a summation of the AZE from each detuned state. This idea is examined by comparing the integrated intensity of the bare cavity with the total AZE predicted by F in Eq. (1) as a function of the $2\gamma_{phase}$. The results are shown in Figs. 3(a) and 3(b) for cases in which the cavity is detuned from all emission lines and tuned to BX^0, respectively. As shown in Fig. 3(a), the prediction made by F is in good agreement with the direct calculation. This confirms that the off-resonant cavity light emission is attributable to the AZE from each detuned state. Moreover, the intensity of the central cavity line in the triplet is also dominated by the AZE from the detuned optically active states of X^+, X^-, and XX^0, as shown in Fig. 3(b). This result directly shows that the central cavity peak in the triplet arises from these detuned states with the help of the AZE. Therefore, the process giving rise to the triplet can be interpreted as follows. When BX^0 is generated by random carrier injection, the interaction with the cavity results in VRS. When the other optically active states X^+, X^-, and XX^0 are generated, the cavity photon can be created by the AZE, and at the same time the optically active states change into single hole, single electron, and BX^0 states, respectively. In this case, the cavity photon cannot form VRS states and the bare cavity lines appear in the spectra. Thus, VRS and the bare cavity lines are generated randomly and the stochastically averaged spectrum results in the triplet.

Although the triplet can be explained as described above, a small difference remains between the direct calculation and the prediction made using F, which suggests the existence of processes other than the AZE. This effect might arise from higher order processes, in which additionally injected carri-

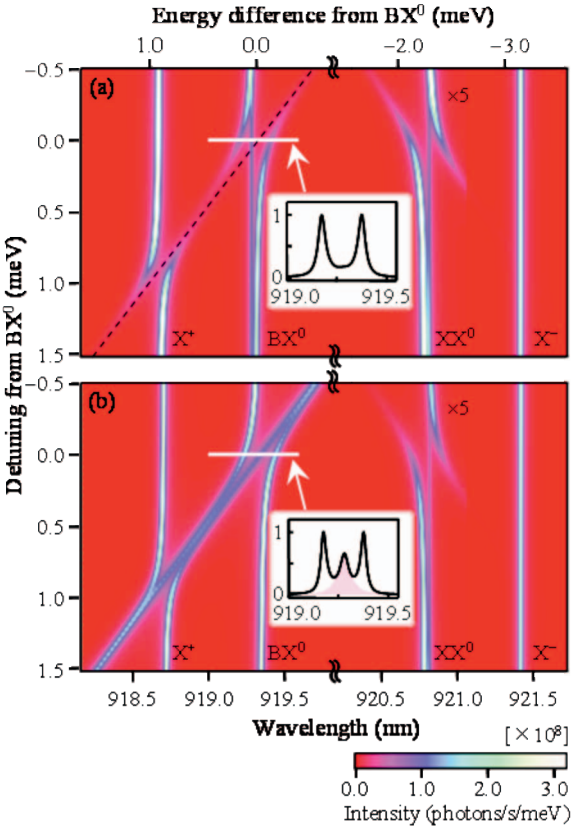

FIG. 2. (Color) Calculated spectra (a) without and (b) with pure dephasing. The dashed line represents the resonant wavelength of the cavity. The spectral resolution is set to $2\gamma_{reso}=30$ μeV in the former case and $2\gamma_{reso}=0$ μeV in the latter to compensate for the difference in line broadening. The color scale around the XX^0 lines (920.5–920.0 nm) has been offset by a factor of five. The insets show the normalized spectra of VRS without the x-polarized components when the detuning from BX^0 is zero.

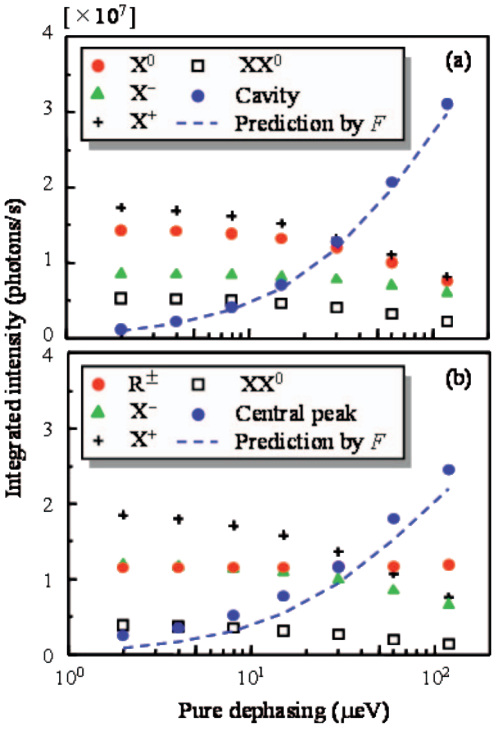

FIG. 3. (Color) Dependence of integrated intensities on the pure-dephasing rate. The cavity is (a) +2.5 meV detuned from BX^0 and (b) tuned to BX^0. The dashed lines are calculated using F with the integrated intensities of the optically active states (BX^0, X^+, X^-, and XX^0) in panel (a) and (X^+, X^-, and XX^0) in panel (b). Here, the AZE from BX^0 is not included in the prediction made using F in panel (b), because BX^0 forms VRS states with the cavity and does not cause the AZE. $R^{\pm}$ represents the intensities of the upper (+) and lower (−) VRS states, and the central peak represents the additional bare cavity peak in VRS.

ers turn BX^0 into the other states while it still interacts with the cavity. This process could occur without the AZE (Appendix B). However, this effect is small under low-excitation conditions [for example, Fig. 2(a)], which is also evidenced by the small size of the deviation from the prediction made using F. Therefore, we conclude that the AZE, as discussed above, is the main process involved in forming the triplet.

Since the origin of the on-resonant triplet has been clarified, we will now discuss the conditions required for observation of the triplet. Although it is difficult to give a general and precise statement due to the large number of factors that it depends on (for example, the pure-dephasing rate and the detuning of each charging state), discussions using a few specific parameters are possible. For this purpose, in Fig. 4 we show the spectra obtained on varying $2\Gamma_{spon}$, $2\Gamma_{cav}$, and g. Here, the other parameters are fixed and the cavity is tuned to BX^0. When we focus on the dependence on $2\Gamma_{spon}$ [Fig. 4(a)], it is found that the middle peak in the triplet becomes smaller when $2\Gamma_{spon}$ is increased. This is because the AZE from the detuned state (X^+, X^-, and XX^0) becomes smaller, as is clear from the definition of F. In practice, $2\Gamma_{spon}$ ranges from 0.044 μeV (15 ns) to 0.66 μeV (1 ns), depending on the existence of the in-plane PBG effect.[16,17] Therefore, one finds by comparing the spectra (the black dashed line and the red line) that the effect of $2\Gamma_{spon}$ is rather small in realistic cases. This means that the existence of the PBG is not critical for observation of the triplet. Next, we discuss the dependence on $2\Gamma_{cav}$ (the cavity Q-factor). As shown in Fig. 4(b), the central peak in the triplet disappears when $2\Gamma_{cav}$ is increased (the cavity Q factor is decreased). One reason for this observation is again a decrease in the AZE. Furthermore, in this case the central peak is hidden to some extent by the broadened VRS peaks. Therefore, it becomes more difficult to observe the triplet. Another effect can be seen when the coupling constant g is changed [Fig. 4(c)]. In this case, the central peak becomes less obvious with a decrease in the energy separation between the VRS peaks as well as a decrease in the AZE. Thus, the conditions necessary to observe the triplet are somewhat complicated. However, our calculations imply that one can observe the triplet only when both the cavity Q factor and the coupling constant g are sufficiently large. From the viewpoint of the coupling constant, this conclusion seems reasonable because the triplet has been observed only when the QD is deterministically embedded at the center of the nanocavity.[7,10,11]

We have now discussed most of the important features for observation of the spectral triplet. However, we must also

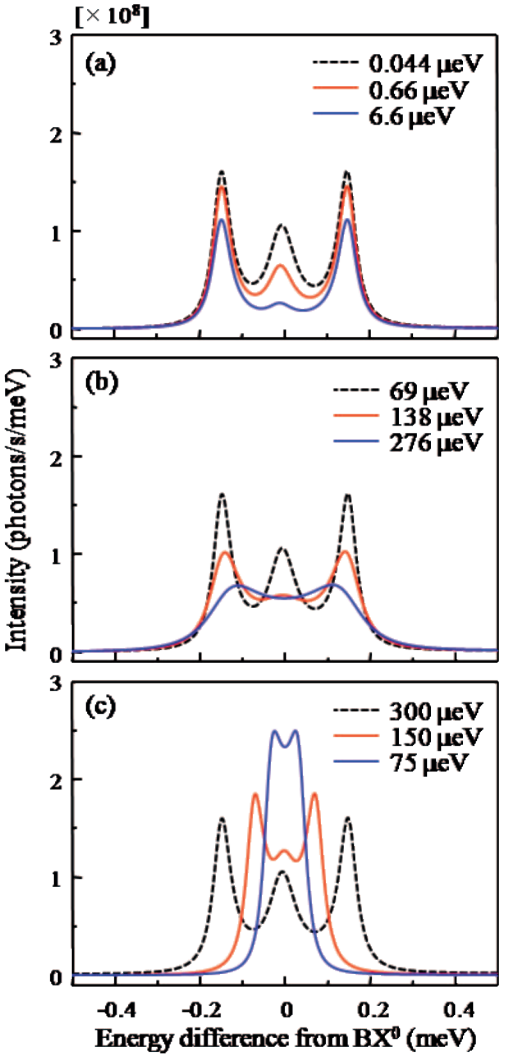

FIG. 4. (Color) Spectral dependence on (a) $2\Gamma_{spon}$, (b) $2\Gamma_{cav}$, and (c) g. In panel (a), the spectra are calculated using $2\hbar\Gamma_{spon}=0.044$ μeV (15 ns), 0.66 μeV (1 ns), and 6.6 μeV (100 ps), respectively. In panel (b), calculations are performed using $2\hbar\Gamma_{cav}=69$ μeV ($Q=20,000$), 138 μeV ($Q=10,000$), and 276 μeV ($Q=5,000$), respectively, and in panel (c), $2\sqrt{2}\hbar g=300$ μeV, 150 μeV, and 75 μeV, respectively. Here, $2\sqrt{2}\hbar g$ corresponds to the energy separation of the vacuum Rabi splitting in our definition. The spectra denoted by the black dashed lines are the same as those in Fig. 2(b).

mention one more important factor, the pump-photon energy. Thus far, optical excitation of the barrier region (GaAs) has been assumed. In other words, the pump-photon energy is *above* the GaAs band-gap energy. Therefore, X^+ and X^- states are generated because a nonequal number of electrons and heavy holes can be injected. However, these X^+ and X^- states are *not* created when the pump-photon energy is *below* the GaAs band-gap energy because electrons and heavy holes are more likely to be injected in pairs than independently.[23,24] Therefore, in this case X^+ and X^- states cannot cause the AZE and the central peak in the triplet disappears in a low-excitation regime. Conversely, in a high-excitation regime, the triplet remains even if the injection of electron-hole pairs is assumed, because the AZE from the

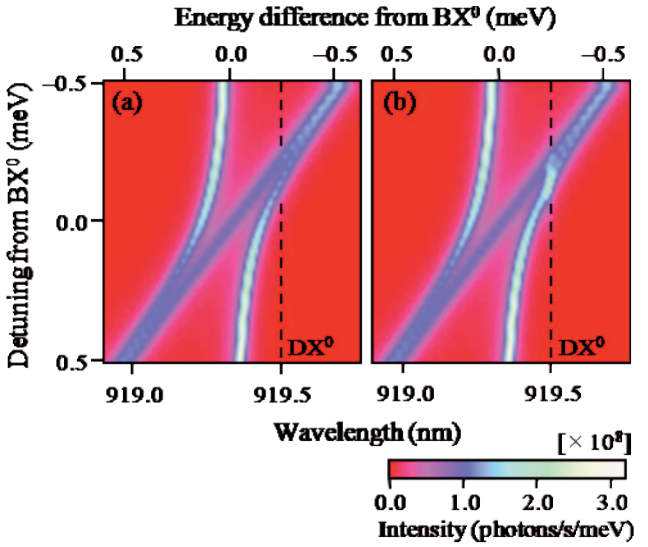

FIG. 5. (Color) Calculated spectra around the BX^0 line (a) without and (b) with an Overhauser field of equal magnitude (20 mT) in the x, y, and z directions. The dashed line is the energy level of DX^0. The spectra for the other values of detuning are the same as in Fig. 2(b).

XX^0 states and higher order processes cannot be negligible (see Appendix C). Consequently, if we limit our discussion to a low-excitation regime, the pump-photon energy has to be above the GaAs band-gap energy to observe the triplet, which is consistent with experiment.[7,10,11] To summarize, the requirements for observation of the triplet have been discussed based on our formalism. In particular, we conclude that the triplet is not a phenomenon peculiar to the 2DPC nanocavity, but can be observed for many different cavity geometries, including micropillars[5] and microdisks[6] when the abovementioned conditions are satisfied. We believe that these predictions will also be proved by experiments in the future.[31]

B. Cavity-mediated mixing

In the previous section we demonstrated that the on-resonant triplet, as well as the off-resonant cavity light emission, is explained well by the AZE from the detuned states in a low-excitation regime. However, a difference remains between the calculation shown in Fig. 2(b) and the experimental findings:[10] the cavity-mediated mixing of the BX^0 and DX^0 states. The spin-flip processes caused by the HF interactions are strong candidates for this phenomenon from an experimental viewpoint. Therefore, we now discuss the effect of HF interactions, which can be modeled by a nuclear magnetic field $\boldsymbol{B}_N=(B_{N,x},B_{N,y},B_{N,z})$ known as the Overhauser field.[32] This field does not affect the heavy-hole pseudospins, so the interaction is described by $H_{hf}=g_e\mu_B(B_{N,x}s_e^x+B_{N,y}s_e^y+B_{N,z}s_e^z)$ with $s_e^x\equiv(s_e^+ + s_e^-)/2$ and $s_e^y\equiv -i(s_e^+ - s_e^-)/2$, where g_e is the electron g factor and μ_B is the Bohr magneton. The Overhauser field is temporally fluctuating in a precise sense, but the correlation time is relatively long (~ 1 ms) and so can be treated as a stochastically dispersed quasistatic field.[32] In the case of InAs/GaAs QDs,

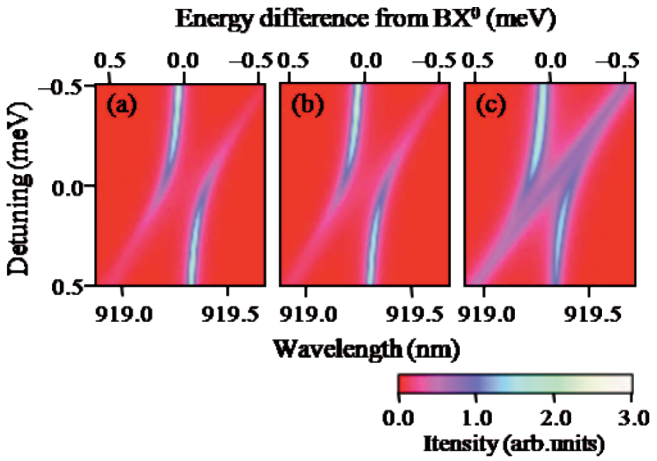

FIG. 6. (Color) Injection rate dependence of $S_{cav}(\omega)+S_y(\omega)$ around the BX^0 line without pure dephasing. The injection rates are (a) 3.3×10^1 neV (5.0×10^7 s^{-1}), (b) 3.3×10^2 neV (5.0×10^8 s^{-1}), and (c) 3.3×10^3 neV (5.0×10^9 s^{-1}). Each color scale is normalized in order to compare the spectral shapes.

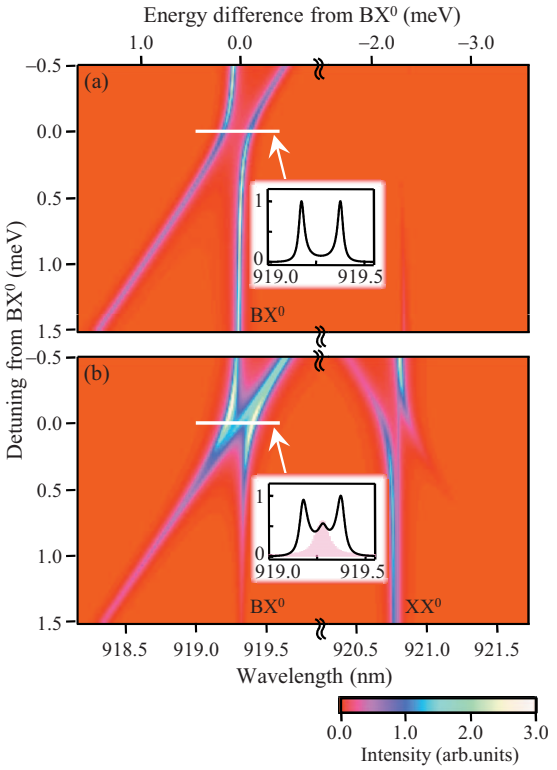

FIG. 7. (Color) Calculated spectra using the injection model for electron-hole pairs. The injection rates are (a) 3.3×10^1 neV (5.0×10^7 s^{-1}) and (b) 6.6×10^3 neV (1.0×10^{10} s^{-1}). Each color scale is normalized in order to compare the spectral shapes. The insets show the normalized spectra for VRS without the x-polarized components when the detuning from BX^0 is zero.

the root-mean-square values for $B_{N,x}$, $B_{N,y}$, and $B_{N,z}$ are in the range 9.5–30 mT. Consequently, the spectra are calculated by adding H_{hf} to $H_S(t)$ for a particular case of the Overhauser field with an equal magnitude of 20 mT in the x, y, and z directions. As shown in Fig. 5, an additional line becomes activated when the Overhauser field is taken into account, corresponding to the cavity-mediated mixing of BX^0 and DX^0. We note that the calculated results are now in good agreement with the experiments.[10] The role of the Overhauser field is explained as follows. The Overhauser field in arbitrary directions breaks the symmetry of $H_S(t)$, and DX^0 is mixed with BX^0.[33,34] Therefore, DX^0 becomes able to interact with photons. However, the Overhauser field is not sufficient to induce non-negligible light emission at the DX^0 energy because of the considerable detuning between DX^0 and BX^0 ($\sim$0.25 meV), which makes the mixing negligible. For the same reason, BX^0 still interacts with photons strongly, and forms VRS states with the cavity when the detuning between the cavity and BX^0 becomes smaller. In this situation, if one of the VRS states is tuned to DX^0, the Overhauser field-induced mixing between the DX^0 and BX^0 components in the VRS states becomes strong because of their resonance. Therefore, the light emission is enhanced when DX^0 is tuned to the VRS state rather than the bare cavity. The hypothesis proposed in Ref. 10 is thus verified theoretically (for further discussion, see Appendix D).

IV. SUMMARY AND CONCLUSION

We have presented a comprehensive theory of the couplings that occur between a nanocavity and exciton complexes in a QD that allows various charge configurations. Our numerically calculated results not only reproduce the unique features of the QD-exciton complexes, but also successfully predict the experimentally observed on-resonant spectral triplet, the origin of which has puzzled the community for several years. By comparing the intensity of the central peak in the triplet with the values predicted by the factor F, we conclude that the on-resonant triplet is explained well by the AZE from the detuned states under a low-excitation regime.

Furthermore, our theory also allows the cavity-mediated mixing of bright and dark exciton states observed in recent experiments to be studied. We have demonstrated that this phenomenon can be reproduced by the effect of Overhauser fields. This confirms that the cavity-mediated mixing is theoretically attributed to HF interactions.

The theory presented here can thus fully and consistently explain recent experimental results. Our formalism should prove to be useful for future studies, such as practical analyses of QIP using QD spins and cavity QED,[1] studies of the design and optimization of the performance of single photon sources,[2] and numerical tests for proposed applications (for example, using the AZE).[15] We believe that our findings will accelerate a full understanding of the physical nature of solid-state cavity QED systems.

ACKNOWLEDGMENT

This work was supported by Research Programs (Grant-in-Aid, Centre of Excellence, and Special Coordination Fund) for Scientific Research from the Ministry of Education, Culture, Sports, Science, and Technology of Japan.

APPENDIX A: CIRCULARLY POLARIZED COMPONENTS

Here, we describe the two circularly polarized components in $S_{\mathrm{spon}}(\omega)$ for convenience. Because similar formalism to that used in the main text can easily be applied to these components, only the result is presented

$$S_{\mathrm{spon}}(\omega) = S_{\mathrm{L}}(\omega) + S_{\mathrm{R}}(\omega), \tag{A1}$$

with

$$S_{\mathrm{L}}(\omega) = \frac{2\Gamma_{\mathrm{spon}}}{\pi}\mathrm{Re}\left[\int_0^\infty \mathrm{d}\tau\langle c_\uparrow^\dagger(t)d_\downarrow^\dagger(t)d_\downarrow(t+\tau)c_\uparrow(t+\tau)\rangle \times\exp(\mathrm{i}\omega\tau-\gamma_{\mathrm{reso}}\tau)\right], \tag{A2}$$

$$S_{\mathrm{R}}(\omega) = \frac{2\Gamma_{\mathrm{spon}}}{\pi}\mathrm{Re}\left[\int_0^\infty \mathrm{d}\tau\langle c_\downarrow^\dagger(t)d_\uparrow^\dagger(t)d_\uparrow(t+\tau)c_\downarrow(t+\tau)\rangle \times\exp(\mathrm{i}\omega\tau-\gamma_{\mathrm{reso}}\tau)\right], \tag{A3}$$

where $S_{\mathrm{L}}(\omega)$ and $S_{\mathrm{R}}(\omega)$ denote the left and right circularly polarized components of $S_{\mathrm{spon}}(\omega)$, respectively.

APPENDIX B: HIGHER-ORDER PROCESSES

In this section, we discuss the small difference between the prediction made using F and the direct calculation shown in Fig. 3(b). In order to identify the physical reason for this occurrence, the injection rate dependence of $S_{\mathrm{cav}}(\omega)+S_y(\omega)$ around the BX^0 line is studied without pure dephasing, as shown in Fig. 6 ($2\gamma_{\mathrm{reso}}=30$ μeV). Here, $S_x(\omega)$ is omitted from the spectra in order to eliminate the confusing x-polarized line. When the injection rate is relatively small [Figs. 6(a) and 6(b)], only the VRS can be seen. However, the additional peak appears again between the VRS peaks when the injection rate is increased [Fig. 6(c)]. Here there is no AZE because the pure dephasing is ignored; higher order processes should therefore become important, because there is a good chance that additional carriers can be injected into the S shells while it still drives the cavity. One possible higher-order process can be considered as follows. When an electron and a heavy hole are injected into the QD, the QD changes into the BX^0 state and it begins to interact with the cavity. The QD then emits a photon into the cavity and is transformed into the ground state (no electron-hole pairs in the QD). If another electron (heavy hole) is injected into the QD at this moment, the QD moves into a single electron (heavy hole) state. In this situation, the QD becomes unable to reabsorb the photon in the cavity because it has to transit from the single electron (heavy hole) state into the $\mathrm{X}^-(\mathrm{X}^+)$ state, but its transition energy is different from the cavity resonance due to the Coulomb interactions. Therefore, the photon in the cavity is directly emitted into free space. Thus, the extra electron (heavy hole) makes it impossible for the QD to reversibly exchange energy with the cavity, resulting in the bare cavity emission. There are of course many other paths by which the higher order processes occur, but these would all be quantitatively similar. The small difference shown in Fig. 3(b) might also arise from these higher order processes. However, as shown in Figs. 6(a) and 6(b), this effect is too small to form the triplet in a low-excitation regime. As a result, we conclude that the dominant factor in formation of the central peak in the triplet shown in Fig. 2(b) is the AZE.

APPENDIX C: INJECTION OF ELECTRON-HOLE PAIRS

In the main text, we discuss the case where electrons and heavy holes are injected independently. This injection model corresponds to optical excitation of the barrier region (GaAs). It has been reported that charged states such as X^+ and X^- are not generated for excitation energies below that of the GaAs band-gap.[23,24] This is because the same number of electrons and holes are injected into the S shells. Therefore, in this section we discuss the case where electrons and heavy holes are injected in pairs. This type of excitation can be modeled by the following Liouvillian:

$$L_{\mathrm{inj,pair}}X \equiv -P\sum_\sigma (d_\sigma c_{-\sigma}c_{-\sigma}^\dagger d_\sigma^\dagger X + X d_\sigma c_{-\sigma}c_{-\sigma}^\dagger d_\sigma^\dagger - 2c_{-\sigma}^\dagger d_\sigma^\dagger X d_\sigma c_{-\sigma}), \tag{C1}$$

where $-\sigma$ denotes the inversion of σ, and the summation of σ is again taken for $\uparrow$ and $\downarrow$. This Liouvillian describes injection of the $+1/2$ $(-1/2)$ spin electron together with the $+3/2$ $(-3/2)$ pseudospin heavy hole, at a rate of $2P$. In other words, bright excitons are injected incoherently.

In Fig. 7 we show the emission spectra calculated using Eq. (C1) instead of Eq. (15). As shown in Fig. 7(a), the X^+ and X^- emission lines are not observed. This is because the X^+ and X^- states are not created by injection of the electron-hole pairs. Furthermore, the carrier injection rate is so low that the XX^0 state is negligible. Therefore, the AZE from the XX^0 state also becomes negligible. As a result, there is an ideal VRS between the cavity and BX^0. Thus, the spectral triplet is not observed in a low-excitation regime when electron-hole pairs are injected.

In contrast, if the carrier injection rate is increased, the AZE from the XX^0 state and higher-order processes cannot be negligible. As a result, the central peak in the triplet emerges again, as shown in Fig. 7(b). This means that the pump-photon energy (above or below the vicinity of the GaAs band-gap energy) influences the features of the central peak in the triplet.

APPENDIX D: BEHAVIOR OF DARK EXCITONS

In the main text, we describe how symmetry breaking induced by the HF interactions makes the DX^0 states illuminant due to mixing with BX^0, which determines the behavior of the DX^0 states. However, it is also important to investigate whether factors (such as strain-induced piezoelectric fields) other than the HF interactions activate the DX^0 states. Here we discuss the optical selection rules for the DX^0 states from the viewpoint of the symmetry of the QD-confinement potential.

When the QD-confinement symmetry belongs to $\boldsymbol{D}_{2d}$ point group symmetry (for example, a cylindrical QD), the exciton states consisting of an electron in the conduction band (Γ_6) and a heavy hole in the valence band (Γ_6) transform according to $\Gamma_6 \otimes \Gamma_6 = \Gamma_1 + \Gamma_2 + \Gamma_5$ in the double group notation.[35] Following a standard method to obtain selection rules in group theory, the Γ_5 is a doublet that is optically active for the light fields polarized in the xy plane, which correspond to BX^0 states. In contrast, the Γ_1 and Γ_2 states are optically inactive singlet states or DX^0 states. In a practical QD, the confinement potential belongs to $\boldsymbol{C}_{2v}$ symmetry. When lowering the symmetry from $\boldsymbol{D}_{2d}$ to $\boldsymbol{C}_{2v}$, the Γ_5 state splits into two states, $\Gamma_5 \rightarrow \Gamma_2 + \Gamma_4$, which are optically active for light fields polarized in the x and y directions, respectively. In a similar manner, $\Gamma_2 \rightarrow \Gamma_3$ and $\Gamma_1 \rightarrow \Gamma_1$ are obtained for DX^0 states. Γ_3 is still optically inactive, whereas Γ_1 becomes optically active for light fields polarized in the z direction.

This result suggests that one of the DX^0 states in the $\boldsymbol{C}_{2v}$ confinement potential can interact with the z-polarized light fields. Therefore, it is possible for the DX^0 state to interact with the cavity field, which might lead to a similar consequence to that shown in Fig. 3(b) when there are z-polarized components in the cavity at the QD position. However, in the case of a 2DPC nanocavity,[18] there is no z component at the center of the 2DPC slab, because a mirror plane is present here. Thus, at least in principle, the DX^0 states in the $\boldsymbol{C}_{2v}$ confinement potential cannot interact with the 2DPC nanocavity without HF interactions when the QD is embedded at the center of the slab.

[1] A. Imamoglu, D. D. Awschalom, G. Burkard, D. P. DiVincenzo, D. Loss, M. Sherwin, and A. Small, Phys. Rev. Lett. **83**, 4204 (1999).

[2] P. Michler, A. Kiraz, C. Becher, W. V. Schoenfeld, P. M. Petroff, E. Lidong Zhang, E. Hu, and A. Imamoğlu, Science **290**, 2282 (2000).

[3] S. Noda, Science **314**, 260 (2006).

[4] T. Yoshie, A. Scherer, J. Hendrickson, G. Khitrova, H. M. Gibbs, G. Rupper, C. Ell, O. B. Shchekin, and D. G. Deppe, Nature (London) **432**, 200 (2004).

[5] J. P. Reithmaier, G. Sęk, A. Löffler, C. Hofmann, S. Kuhn, S. Reitzenstein, L. V. Keldysh, V. D. Kulakovskii, T. L. Reinecke, and A. Forchel, Nature (London) **432**, 197 (2004).

[6] K. Srinivasan and O. Painter, Nature (London) **450**, 862 (2007).

[7] K. Hennessy, A. Badolato, M. Winger, D. Gerace, M. Atatüre, S. Gulde, S. Fält, E. L. Hu, and A. Imamoglu, Nature (London) **445**, 896 (2007).

[8] D. Press, S. Götzinger, S. Reitzenstein, C. Hofmann, A. Löffler, M. Kamp, A. Forchel, and Y. Yamamoto, Phys. Rev. Lett. **98**, 117402 (2007).

[9] M. Kaniber, A. Laucht, A. Neumann, J. M. Villas-Bôas, M. Bichler, M.-C. Amann, and J. J. Finley, Phys. Rev. B **77**, 161303(R) (2008).

[10] M. Winger, A. Badolato, K. J. Hennessy, E. L. Hu, and A. Imamoglu, Phys. Rev. Lett. **101**, 226808 (2008).

[11] A. Badolato, M. Winger, K. J. Hennessy, E. L. Hu, and A. Imamoglu, C. R. Phys. **9**, 850 (2008).

[12] M. Nomura, Y. Ota, N. Kumagai, S. Iwamoto, and Y. Arakawa, Appl. Phys. Express **1**, 072102 (2008).

[13] Y. Ota, M. Shirane, M. Nomura, N. Kumagai, S. Ishida, S. Iwamoto, S. Yorozu, and Y. Arakawa, Appl. Phys. Lett. **94**, 033102 (2009).

[14] M. Yamaguchi, T. Asano, and S. Noda, Eighth International Conference on Physics of Light-Matter Coupling in Nanostructures, Tokyo, Japan, 7–11 April 2008 (unpublished).

[15] M. Yamaguchi, T. Asano, and S. Noda, Opt. Express **16**, 18067 (2008).

[16] M. Fujita, S. Takahashi, Y. Tanaka, T. Asano, and S. Noda, Science **308**, 1296 (2005).

[17] K. Kounoike, M. Yamaguchi, M. Fujita, T. Asano, J. Nakanishi, and S. Noda, Electron. Lett. **41**, 1402 (2005).

[18] Y. Akahane, T. Asano, B. S. Song, and S. Noda, Nature (London) **425**, 944 (2003).

[19] A. Naesby, T. Suhr, P. T. Kristensen, and J. Mørk, Phys. Rev. A **78**, 045802 (2008).

[20] K. Srinivasan and O. Painter, Phys. Rev. A **75**, 023814 (2007).

[21] F. P. Laussy, E. del Valle, and C. Tejedor, Phys. Rev. Lett. **101**, 083601 (2008).

[22] S. Hughes and P. Yao, Opt. Express **17**, 3322 (2009).

[23] J. J. Finley, A. D. Ashmore, A. Lemaitre, D. J. Mowbray, M. S. Skolnick, I. E. Itskevich, P. A. Maksym, M. Hopkinson, and T. F. Krauss, Phys. Rev. B **63**, 073307 (2001).

[24] E. S. Moskalenko, K. F. Karlsson, P. O. Holtz, B. Monemar, W. V. Schoenfeld, J. M. Garcia, and P. M. Petroff, Phys. Rev. B **64**, 085302 (2001).

[25] H. W. van Kesteren, E. C. Cosman, W. A. J. A. van der Poel, and C. T. Foxon, Phys. Rev. B **41**, 5283 (1990).

[26] R. Seguin, A. Schliwa, S. Rodt, K. Pötschke, U. W. Pohl, and D. Bimberg, Phys. Rev. Lett. **95**, 257402 (2005).

[27] M. Bayer, G. Ortner, O. Stern, A. Kuther, A. A. Gorbunov, A. Forchel, P. Hawrylak, S. Fafard, K. Hinzer, T. L. Reinecke, S. N. Walck, J. P. Reithmaier, F. Klopf, and F. Schäfer, Phys. Rev. B **65**, 195315 (2002).

[28] H. J. Carmichael, R. J. Brecha, M. G. Raizen, H. J. Kimble, and P. R. Rice, Phys. Rev. A **40**, 5516 (1989).

[29] C. Ginzel, H. J. Briegel, U. Martini, B. G. Englert, and A. Schenzle, Phys. Rev. A **48**, 732 (1993).

[30] S. Rodt, A. Schliwa, K. Pötschke, F. Guffarth, and D. Bimberg, Phys. Rev. B **71**, 155325 (2005).

[31] S. Hughes *et al.* have recently studied the same phenomena (i.e., the off-resonant cavity emission and the spectral triplet) through the Green's function formalism.[22] In their work, it is concluded that the off-resonant cavity emission from other detuned states is so much less than the on-resonant VRS that this mechanism is unlikely to be responsible for the central peak in the triplet. In our view, the essential difference between our model and their model is the treatment of linewidth broadening. In their model, an additional radiative (population) decay is utilized to represent the linewidth broadening while a pure dephasing (broadening without population decay) is utilized in our model. For example,

when Hughes *et al.* present a typical linewidth broadening of 40 μeV, it is accompanied by an additional population decay with a decay rate of $\sim$33 ps, which is very fast compared to the typical lifetime of the QD ($1\sim15$ ns). Here, we limit ourselves to stating that this additional decay process accounts for a large part of the energy, and possibly leads to the different conclusion.

[32] J. Dreiser, M. Atatüre, C. Galland, T. Müller, A. Badolato, and A. Imamoglu, Phys. Rev. B **77**, 075317 (2008).

[33] M. Bayer, O. Stern, A. Kuther, and A. Forchel, Phys. Rev. B **61**, 7273 (2000).

[34] The symmetry of the Hamiltonian is broken by $B_{N,x}$ and $B_{N,y}$ but is not changed by $B_{N,z}$. Therefore, the mixing of BX^0 and DX^0 does not occur regardless of $B_{N,z}$ when $B_{N,x}=B_{N,y}=0$. However, the Overhauser field is temporally fluctuating and cannot keep $B_{N,x}=B_{N,y}=0$ beyond the correlation time ($\sim$1 ms) in most cases. In this context, it is reasonable to discuss the symmetry based on the presence of $B_{N,x}$, $B_{N,y}$, and $B_{N,z}$ corresponding to their root-mean-square values.

[35] E. L. Ivchenko and G. E. Pikus, *Superlattices and Other Heterostructures*, Springer Series in Solid-State Sciences Vol. 110 (Springer-Verlag, Berlin, 1997).